(Received 30 September 2025, Accepted 1 December 2025, Scheduled 16 December 2025)

Compact Millimeter-Wave Microstrip Dual-Band Filter Using the Ring Type Structure

Wei Zhao[1,*], Mingen Tian[1], Ziyan Lu[1], Hailong Wang[1], Yiming Zhang[2], and Huali Zhu[2]

[1] *Southwest Electronic Equipment Research Institute, Chengdu 610036, Sichuan, China*
[2] *University of Electronic Science and Technology of China, Chengdu 611731, Sichuan, China*

ABSTRACT: A compact microstrip dual-band filter using stepped-impedance resonators (SIRs) is proposed. The ring-type structure is used to minimize the size of the filter, and the location of the input/output excitation port is used to adjust the filter's performance. A dual-band filter has been fabricated and measured to verify the performance of the proposed configuration. The results show that the filter exhibits two passbands, centered at 30.5 GHz and 35.9 GHz, with fractional bandwidths of 7.2% and 5.6%, respectively. The corresponding insertion losses at the center frequencies are 2.7 dB and 3.3 dB. The proposed filter configuration shows great potential for applications in next-generation 5G and satellite communication systems requiring compact and high-performance multi-band filters.

1. INTRODUCTION

The demand for dual-band operation has been growing fast with the rapid development of wireless communication systems. As the core circuitry of multi-channel communication systems, multi-channel filters and multiplexers have been proposed and extensively studied by scholars worldwide. Various structural configurations have been developed to achieve effective multi-channel filtering [1–5].

The initial approach adopted a cascaded configuration of power dividers and filters [6]. This structure is not only simple in topology but also allows the independent design of each channel filter, facilitating high channel selectivity and strong inter-channel isolation. However, its relatively large size poses a significant challenge for device miniaturization. To address limitation and achieve more compact designs, multi-channel filters based on multi-mode resonators (MMRs) have been proposed. MMRs are generally categorized into two types: stub-loaded resonators and ring-based or other planar geometric resonators. The former utilizes stub reuse to generate multiple resonant modes [7], while the latter typically introduces perturbations through techniques such as stub loading, partial etching, and asymmetric feeding, thereby separating the originally degenerate orthogonal modes to form multiple resonant modes [8]. Dual-channel or multi-channel filters based on multi-mode resonators enable miniaturized designs, making them particularly suitable for portable devices, and this approach has become the mainstream solution for multi-channel filter design.

Moreover, stepped impedance resonators (SIRs) are also commonly used elements in microwave circuit design. Compared to uniform impedance resonators (UIRs), SIRs offer greater design flexibility. Due to their nonuniform line widths, the multiple frequency distribution can be controlled by adjusting the impedance ratio. They are frequently employed in half-wavelength and quarter-wavelength resonator configurations, often enabling ultra-wideband performance and wide stopband characteristics [9–12]. In multi-mode resonator designs, incorporating a stepped impedance structure allows adjustment of transmission poles and zeros, thereby facilitating tailored bandwidth and channel selectivity [13–16].

This paper presents a millimeter-wave dual-channel filter based on dual-mode resonators. An asymmetric capacitive coupling feed structure is adopted, which not only meets the required external quality factor (Q factor) for the dual-channel filter but also introduces cross-coupling that generates a pair of transmission zeros, significantly enhancing the selectivity of the high-frequency channel. Furthermore, the two dual-mode resonators are arranged in a compact ring-based layout, contributing to the miniaturization of the device.

2. ANALYSIS OF THE DUAL-MODE RESONATORS

2.1. Analysis of Resonant Frequency versus Admittance Ratio and Electrical Length Ratio in the T-Shaped Dual-Mode Resonator

The initial analysis is conducted on a simple T-shaped dual-mode resonator, as illustrated in Fig. 1(a). For generality, the admittance and electrical length of the symmetric stubs are defined as variables and set to m times and n times of those of the vertical stub, respectively. Owing to the symmetrical structure of the T-shaped resonator, even- and odd-mode analysis can be applied. Under odd-mode excitation, the symmetry plane functions as a perfect electric wall (short-circuited to ground), and the corresponding equivalent circuit is shown in Fig. 1(b). Under even-mode excitation, the symmetry plane acts as a perfect magnetic wall (open-circuited), with the equivalent circuit depicted in Fig. 1(c).

* Corresponding author: Wei Zhao (weizhao_cn@163.com).

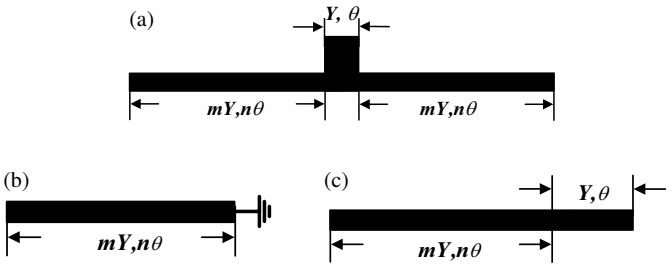

FIGURE 1. (a) T-shaped dual-mode resonator, (b) odd-mode equivalent circuit, (c) even-mode equivalent circuit.

Based on transmission line theory, the input admittance (Y_{in}) of a microstrip line is:

$$Y_{in} = Y_0 \frac{Y_L + jY_0 \tan\theta}{Y_0 + jY_L \tan\theta} \tag{1}$$

where Y_0 and θ represent the characteristic admittance and electrical length of the microstrip line, respectively, and Y_L denotes the load admittance. Thus, the input admittances of the odd- and even-mode equivalent circuits are:

$$\begin{cases} Y_{in}^o = -jmY \cot n\theta \\ Y_{in}^e = j\frac{1}{2}Y \frac{m\tan n\theta + \frac{1}{2}\tan\theta}{\frac{1}{2} - m\tan\theta\tan n\theta} \end{cases} \tag{2}$$

Applying the resonance conditions ($Y_{in} = 0$) to Eq. (2) yields Eq. (3).

$$\begin{cases} \cot n\theta = 0 \\ \frac{2m\tan n\theta + \tan\theta}{1 - 2m\tan\theta\tan n\theta} = 0 \end{cases} \tag{3}$$

First, the relationship between the resonant modes and admittance is analyzed. By setting $n = 1$ and treating m as a variable, the solutions for the odd and even modes are derived as Eq. (4).

$$\begin{cases} \cot\theta = 0 \\ \frac{\tan\theta}{1-2m\tan^2\theta} = 0 \end{cases} \rightarrow \begin{cases} \theta = (2k+1)\frac{\pi}{2}, & k = 0,1,2,3,\ldots \\ \theta = k\pi, & k = 0,1,2,3,\ldots \end{cases} \tag{4}$$

Revealing that the solutions are independent of m, leading to the first conclusion: the two modes of the T-shaped dual-mode resonator are independent of the microstrip line width. Since only the fundamental frequency is of interest here, although the solutions are infinite in number, only the minimum value is taken ($k = 0$). The correspondence between the physical length and electrical length of the microstrip line is given by Eq. (5).

$$\theta = \frac{2\pi f L\sqrt{\varepsilon_r}}{c} \tag{5}$$

where f is the operating frequency, L the physical length of the microstrip line, ε_r the relative permittivity of the substrate, and c the speed of light. Substituting the minimum solution from Eq. (4) into Eq. (5), the resonant frequencies (f_o, f_e) for the odd and even modes are obtained as shown in Eq. (6).

$$\begin{cases} f_o = \frac{c}{4L\sqrt{\varepsilon_r}} \\ f_e = \frac{c}{2(2L)\sqrt{\varepsilon_r}} \end{cases} \rightarrow f_o = f_e \tag{6}$$

Next, the relationship between the resonant modes and electrical length is analyzed. By setting $m = 1$ and treating n as a variable, the resonance conditions for different values of n are expressed by Eq. (7), and the corresponding solutions are given in Eq. (8).

$$\begin{cases} \cot n\theta = 0 \\ \frac{2\tan n\theta + \tan\theta}{1 - 2\tan\theta\tan n\theta} = 0 \end{cases} \rightarrow \begin{cases} n=1: \begin{cases} \cot\theta = 0 \\ \frac{\tan\theta}{1-2\tan^2\theta} = 0 \end{cases} \\ n=2: \begin{cases} \cot 2\theta = 0 \\ \frac{2\tan 2\theta + \tan\theta}{1-2\tan\theta\tan 2\theta} = 0 \end{cases} \\ n=3: \begin{cases} \cot 3\theta = 0 \\ \frac{2\tan 3\theta + \tan\theta}{1-2\tan\theta\tan 3\theta} = 0 \end{cases} \\ n=4: \begin{cases} \cot 4\theta = 0 \\ \frac{2\tan 4\theta + \tan\theta}{1-2\tan\theta\tan 4\theta} = 0 \end{cases} \\ n=5: \begin{cases} \cot 5\theta = 0 \\ \frac{2\tan 5\theta + \tan\theta}{1-2\tan\theta\tan 5\theta} = 0 \end{cases} \end{cases} \tag{7}$$

$$\begin{cases} n=1: \begin{cases} \theta = \frac{\pi}{2}(2k+1), & k = 0,1,2,3,\ldots \\ \theta = k\pi, & k = 0,1,2,3,\ldots \end{cases} \\ n=2: \begin{cases} \theta = \frac{\pi}{4}(2k+1), & k = 0,1,2,3,\ldots \\ \theta = k\pi, & \arctan\sqrt{5} + k\pi, \\ & k = 0,1,2,3,\ldots \end{cases} \\ n=3: \begin{cases} \theta = \frac{\pi}{6}(2k+1), & k = 0,1,2,3,\ldots \\ \theta = k\pi, & \arctan\sqrt{\frac{7}{5}} + k\pi, \\ & k = 0,1,2,3,\ldots \end{cases} \\ n=4: \begin{cases} \theta = \frac{\pi}{8}(2k+1), & k = 0,1,2,3,\ldots \\ \theta = k\pi, & \arctan(\sqrt{5} \pm \sqrt{2}) + k\pi, \\ & k = 0,1,2,3,\ldots \end{cases} \\ n=5: \begin{cases} \theta = \frac{\pi}{10}(2k+1), & k = 0,1,2,3,\ldots \\ \theta = k\pi, & \arctan\sqrt{\frac{15\pm 2\sqrt{37}}{7}} + k\pi, \\ & k = 0,1,2,3,\ldots \end{cases} \end{cases} \tag{8}$$

Similarly, only the minimum solution is considered and substituted into Eq. (5). For convenience of calculation, with L set to 10 mm, the results are summarized in Table 1 and graphically represented in Fig. 2. It can be observed that as n increases, the f_o and f_e decrease rapidly, with f_o eventually becoming lower than f_e. And when n tends to infinity, $f_e = 2f_o$.

TABLE 1. Resonant frequencies corresponding to different values of n.

f \ *n*	1	2	3	4	5
f_o (GHz)	5.07	1.27	0.56	0.32	0.2
f_e (GHz)	5.07	1.25	0.71	0.45	0.3

2.2. Design of a Stepped-Impedance T-Shaped Dual-Mode Resonator

The stepped impedance resonator proposed in this work is illustrated in Fig. 3. To facilitate the design, both the admittance and electrical length of the stub lines are set to integer multiples. Based on the odd-mode equivalent circuit shown in Fig. 3(c), the input admittance can be expressed as:

$$Y_{in}^o = j3Y \frac{3\tan\theta - \frac{1}{\tan 4\theta}}{3 + \frac{\tan\theta}{\tan 4\theta}} \tag{9}$$

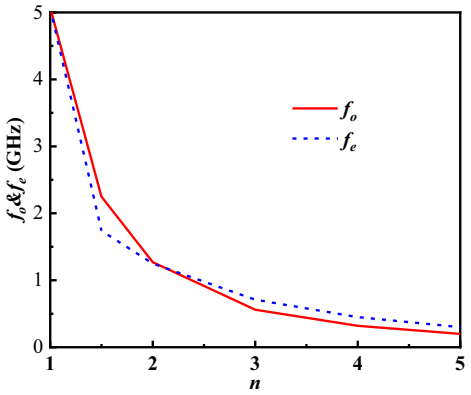

FIGURE 2. Variation of f_o and f_e with respect to n. At this point, the resonant frequencies of the odd and even modes are equal. This leads to the second conclusion: the resonant frequency of a symmetric resonator is equal to that of its odd-mode equivalent circuit.

When the resonance condition is satisfied ($Y_{in} = 0$), the solution is derived as

$$\theta_1 = \arctan\left(\pm\sqrt{\frac{9 \pm 2\sqrt{17}}{13}}\right) + k\pi, \quad k = 0, 1, 2, 3, \ldots \quad (10)$$

By taking the minimum value corresponding to the fundamental frequency as 0.075π and setting $L_1 = 1$ mm, substitution into Eq. (5), we obtain $f_o = 7.6$ GHz. Consequently, $4f_o = 30.4$ GHz, which corresponds to the center frequency of the first channel.

The even-mode equivalent circuit of the stepped impedance resonator is depicted in Fig. 3(d). Due to its composition of three microstrip line sections, directly calculating the input admittance becomes considerably complex. According to the second conclusion established in the previous analysis, the resonant frequency of this circuit is equal to that of its odd-mode equivalent circuit. The odd-mode equivalent circuit of the even-mode equivalent circuit is illustrated in Fig. 3(e), and its input admittance is derived as:

$$Y_{in}^{e\text{-}o} = j3Y\frac{3\tan\theta - \frac{1}{\tan 2\theta}}{3 + \frac{\tan\theta}{\tan 2\theta}} \quad (11)$$

Similarly, when the resonance condition is satisfied ($Y_{in} = 0$), the solution is derived as

$$\theta_2 = \arctan\left(\pm\frac{1}{\sqrt{7}}\right) + k\pi, \quad k = 0, 1, 2, 3, \ldots \quad (12)$$

By substituting the minimum value corresponding to the fundamental frequency, 0.115π, and $L_1 = 1$ mm into Eq. (5), $f_e = 11.66$ GHz is obtained. Consequently, $3f_e = 35$ GHz, which corresponds to the center frequency of the second channel. With a physical length of 1 mm per unit electrical length θ, the design satisfies the required center frequencies for both channels. Here, by adjusting the θ of loaded stubs, center frequencies of the two passbands can be tuned.

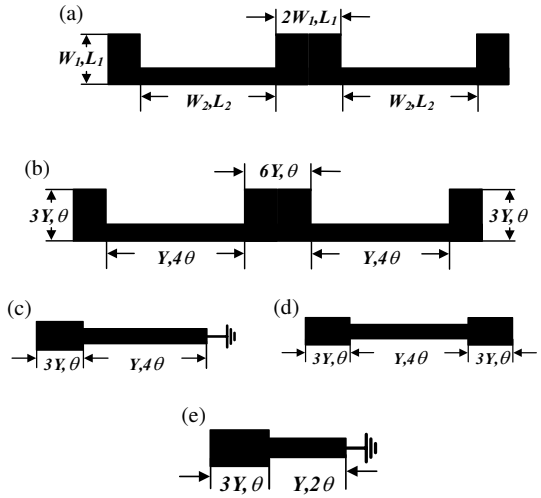

FIGURE 3. (a) Physical layout of the stepped impedance resonator; (b) electrical length distribution of the stepped impedance resonator, (c) odd-mode equivalent circuit, (d) even-mode equivalent circuit, (e) odd-mode equivalent circuit of the even-mode equivalent circuit.

3. DESIGN AND TESTING OF THE DUAL-BAND FILTER

The dual-channel filter is designed on a single-layer Rogers RT/Duroid 5880 substrate with a relative dielectric constant of 2.2 and a thickness of 0.254 mm. The center frequencies of the two channels are designed at $f_L = 30.5$ GHz and $f_H = 35$ GHz, with bandwidths of $BW_L = 2.2$ GHz and $BW_H = 2$ GHz, respectively. The filter structure consists of two dual-mode resonators, where the lower passband is generated by coupling between the odd-mode resonances (f_o) of the two resonators, while the upper passband is formed by coupling between their even-mode resonances (f_e). The corresponding coupling scheme is illustrated in Fig. 4, where solid and dashed lines denote electrical and magnetic coupling, respectively, and "S" and "L" refer to the source and load. The overall physical layout of the filter is presented in Fig. 5.

The operating bandwidth of the two channels is optimized by adjusting the coupling gap between the dual-mode resonators and the width W_1 of the microstrip line. The final dimensions for the coupling gap and microstrip line width (W_1) were determined to be 0.1 mm and 0.5 mm, respectively. The corresponding characteristic impedance of the microstrip line is 65.8 Ω. Meanwhile, the insertion loss is improved by tuning both the coupling gap and the relative position between the port excitation and the resonator.

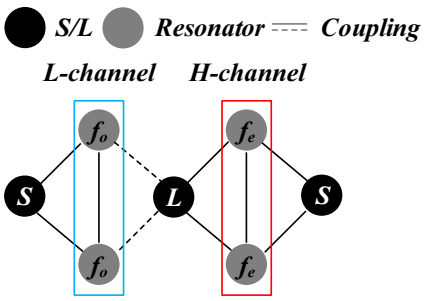

FIGURE 4. Coupling topology.

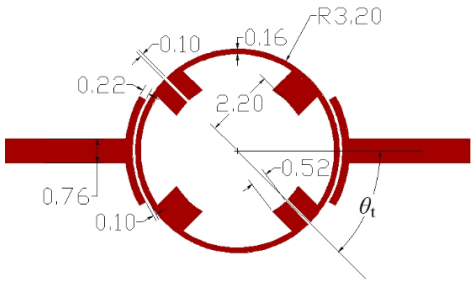

FIGURE 5. Geometry structure of the proposed filter (all unit is mm).

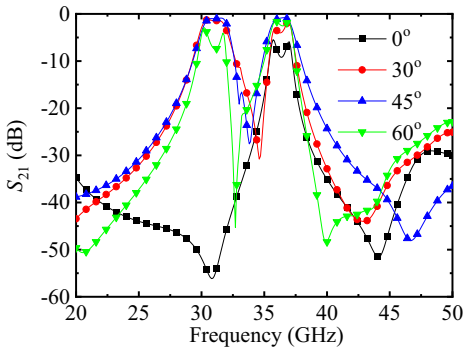

FIGURE 6. Simulated insertion losses with different $\theta_t = 0°, 30°, 45°$ and $60°$.

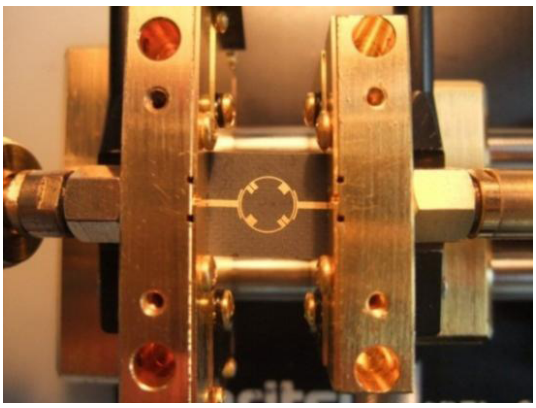

FIGURE 7. Photograph of the dual-band filter (14.6 mm × 12 mm) with the test fixture.

When the coupling gap is 0.1 mm, the simulated insertion losses with different locations ($\theta_t = 0°$, $30°$, $45°$ and $60°$) are shown in Fig. 6. When 45° feed-in input/output ports are employed, the dual-band filter achieves its flattest response and lowest insertion loss. Specifically, the insertion losses are measured at 1 dB and 0.8 dB at the two center frequencies of 31.1 GHz and 36.4 GHz, respectively.

A photograph of the fabricated filter is shown in Fig. 7. The filter is measured by an R&S ZVA67 vector network analyzer with an Anritsu network analyzer universal test fixture up to 40 GHz. As shown in Fig. 8, the results indicate that the two measured passbands are centered at 30.5 GHz and 35.9 GHz, with fractional bandwidths of 7.2% and 5.6%, respectively. The corresponding insertion losses at the center frequencies are

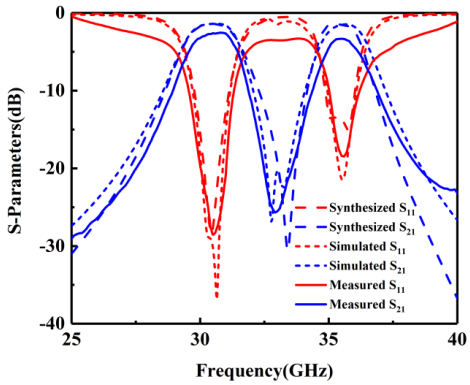

FIGURE 8. Measured results of the proposed filter.

2.7 dB and 3.3 dB. Compared with the simulated results, the insertion losses are becoming larger. These could be attributed to the influence of the test fixture, which cannot be calibrated in the test system. Despite these, the proposed dual-band filter is still an effective configuration with compact size and easy fabrication, which has many attractive characteristics.

4. CONCLUSIONS

A novel dual-band filter based on a ring resonator structure is presented in this paper. A prototype operating in the Ka-band (26.5–40 GHz) has been designed, fabricated, and measured, demonstrating favorable performance. The proposed filter exhibits advantages of structural simplicity, compact size, and straightforward fabrication, making it highly suitable for application in next-generation satellite communication systems — particularly in high-throughput Ka-band links and LEO satellite constellations — as well as in 5G/6G millimeter-wave front-ends operating in corresponding frequency ranges (27.5–28.35 GHz, 35 GHz).

ACKNOWLEDGEMENT

This work was supported by Sichuan Province Engineering Research Center for Broadband Microwave Circuit High Density Integration, and Natural Science Foundation of Sichuan Province under Grant 2025ZNSFSC1444.

REFERENCES

[1] Tang, W. S., Y.-M. Zhang, S. Y. Zheng, and Y. M. Pan, "Low-cost compact inline single-/dual-band filters based on dual-mode dielectric resonators with highly integrated and flexible mixed couplings," *IEEE Transactions on Microwave Theory and Techniques*, Vol. 73, No. 9, 6589–6602, Sep. 2025.

[2] Rao, J., P. Ding, Y. Yu, L. Zhang, and P. Vaitukaitis, "Design of controllable dual-band bandpass filter based on dual-mode metal plate coupled resonator," *IEEE Microwave and Wireless Technology Letters*, Vol. 35, No. 7, 953–956, Jul. 2025.

[3] Xie, W.-B., Y.-H. Ma, D.-W. Wang, C.-H. Yu, Y. Hu, and W.-S. Zhao, "Compact single-and dual-band balanced high-selectivity bandpass filters based on microstrip resonator loaded substrate integrated waveguide," *IEEE Transactions on Electromagnetic Compatibility*, Vol. 67, No. 5, 1629–1633, Oct. 2025.

[4] Huang, X., W. Feng, K. Tang, Y. Cao, W. Che, and Q. Xue, "Miniaturized dual-band filter using D-CRLH resonators with wide stopband and controllable frequencies/bandwidths," *IEEE Microwave and Wireless Technology Letters*, 1–4, 2025.

[5] Lu, L.-X., W.-X. Wang, L. Ma, W.-W. Yang, W. Qin, and J.-X. Chen, "Dual-band bandpass filter based on dual-ridged dual-mode dielectric waveguide resonator," *IEEE Microwave and Wireless Technology Letters*, Vol. 35, No. 10, 1462–1465, Oct. 2025.

[6] Li, J.-L., P. Liu, and J.-H. Ye, "Compact dual-mode loop resonators for microwave triplexer applications," *Journal of Electrical Engineering*, Vol. 74, No. 4, 277–281, 2023.

[7] Song, K., L. Fang, Q. Li, and Y. Fan, "Compact eight-channel diplexer based on quad-mode stepped impedance resonator," *International Journal of Microwave and Wireless Technologies*, Vol. 16, No. 10, 1713–1721, 2024.

[8] Faghir Mirnezami, S. P., M. Tavakoli, F. Setoudeh, and A. Horri, "Design of a triple band-pass balanced filter based on single-stepped-impedance ring resonator with ultra-wide stopband bandwidth," *ETRI Journal*, 1–11, 2025.

[9] Shao, C., R. Cai, X. Zhang, and K. Xu, "Novel compact wideband bandpass filters with high upper stopband rejection featuring a quadruple-mode resonator," *Progress In Electromagnetics Research Letters*, Vol. 125, 37–41, 2025.

[10] Zhou, L., J. Jiang, W. Zhang, P. K. J. Wong, B. Xia, D. Zhang, X. Bai, and X. Lu, "Design of high order HTS duplexer based on SIR structure," *IEEE Transactions on Applied Superconductivity*, Vol. 33, No. 4, 1–8, 2023.

[11] Li, W. T., H. R. Zhang, X. J. Chai, Y. Q. Hei, J. C. Mou, and X. W. Shi, "Compact dual-band balanced-to-unbalanced filtering power divider design with extended common-mode suppression bandwidth," *IEEE Microwave and Wireless Components Letters*, Vol. 32, No. 6, 511–514, 2022.

[12] Yang, L., C. Lu, J. Wang, S. Li, H. Zhao, and X. Yin, "Postwall-slotline stepped impedance resonator and its application to bandpass filter with improved upper stopband," *Electronics*, Vol. 11, No. 6, 851, 2022.

[13] Weng, X.-Y., K.-D. Xu, Y.-J. Guo, A.-X. Zhang, and Q. Chen, "High-selectivity bandpass filter based on two merged ring resonators," *Radioengineering*, Vol. 30, No. 3, 504–509, 2021.

[14] Shankar, E., K. V. P. Kumar, V. K. Velidi, and S. Koziel, "Miniaturized dual-band bandpass filter with wide inter stopband for 5G applications," *IEEE Transactions on Circuits and Systems II: Express Briefs*, Vol. 71, No. 10, 4461–4465, 2024.

[15] Li, Q., J. Fang, W. Cao, J. Sun, J. Ding, W. Tie, F. Wei, C. Zhai, and J. Wu, "Optimization and design of balanced BPF based on mixed electric and magnetic couplings," *Electronics*, Vol. 12, No. 9, 2125, 2023.

[16] Gorur, A. K., A. Turkeli, C. Karpuz, and A. Gorur, "Design of a compact microstrip quadruplexer with closely spaced switchable and tunable channels based on asymmetrical dual-mode loop resonators," *AEU — International Journal of Electronics and Communications*, Vol. 127, 153421, 2020.